Investigation of a High-efficiency and High-frequency 10-kW/800-V Three-phase PWM Converter with Direct Power Factor Control

Roman Barlik, Piotr Grzejszczak, Bernard Leszczyński, and Marek Szymczak

Abstract—The paper presents a concept of a control system for a high-frequency three-phase PWM grid-tied converter (3x400 V / 50 Hz) that performs functions of a 10-kW DC power supply with voltage range of 600÷800 V and of a reactive power compensator. Simulation tests (in PLECS) allowed proper selection of semiconductor switches between fast IGBTs and silicon carbide MOSFETs. As the main criterion minimum amount of power losses in semiconductor devices was adopted. Switching frequency of at least 40 kHz was used with the aim of minimizing size of passive filters (chokes, capacitors) both on the AC side and on the DC side. Simulation results have been confirmed in experimental studies of the PWM converter, the power factor of which (inductive and capacitive) could be regulated in range from 0.7 to 1.0 with *THD$_i$* of line currents below 5% and energy efficiency of approximately 98.5%. The control system was implemented in Texas Instruments TMS320F28377S microcontroller.

Keywords—Three-phase PWM rectifier, reactive power compensator, silicon carbide MOSFET, bidirectional power flow, direct power control (DPC), DC voltage regulation, power factor correction (PFC), LCL filter

I. INTRODUCTION

THE newest power transistors like IGBTs or silicon carbide MOSFETs can be used in high-switching-frequency and high-power converters. Over the last few years the wide band gap (WBG) devices have been becoming increasingly important, because their blocking voltage values of over 1 kV allow them to be used in three-phase grid-tied converters at 3x400 V and 50 Hz [1][2][3][4]. Due to high achievable switching frequency and low power losses in SiC MOSFETs, useful properties of the converter are also obtained, such as high power density, small grid filter dimensions, high energy efficiency and small distortions of the grid currents [5][6].

This creates unprecedented possibilities of using power converters in the power system on a large scale. Particularly important applications of WBG converters are: renewable energy sources (RES) [7][8], improvement of power system quality parameters (active filters) [9][10], integration of consumers and energy sources with different parameters in smart grids (solid state transformers - SST [11][12]) and EV chargers [13][14].

The paper presents selected design problems and experimental investigations of a bidirectional three-phase grid-tied converter with a power level of 10 kW and a 600÷800 V DC voltage range. The main task of the converter is to supply DC power with a unity power factor; however, the system can also be used as a reactive power compensator with adjustable power factor and as a coupling link between the power system and energy storage system in voltage range from 600 to 800 V.

Selection of the main components like power transistors or AC and DC filter, as well as control system with direct power factor correction, were evaluated through simulation studies. The main condition for the selection of power switches from the available IGBTs and silicon carbide MOSFETs was to minimize switching and conduction power losses with the assumption of the switching frequency of at least 40 kHz.

Simulation results and analytical calculations were verified in experimental studies, where the prototype of the converter with SiC transistors was tested. The developed control system allows to set the DC voltage value as well as to directly adjust power factor value in the range from 0.7 to 1.0. In experimental measurements of switching power losses, oscilloscope observations and measurements with power analyzer were used [15]. System has also been tested in the inverter mode, i.e. when transferring energy from the DC side to the AC side.

II. ANALYTICAL AND SIMULATION STUDIES

Table I presents the most important design assumptions for the bidirectional three-phase PWM converter. The electrical scheme of the system, developed for the simulation in the PLECS environment, is shown in Fig. 1. A two-level PWM converter is characterized by a simple construction and a small number of semiconductor devices, but it requires the use of larger passive components to obtain currents and voltages with lower values of total harmonic distortion compared to multi-level topologies.

TABLE I
DESIGN PARAMETERS

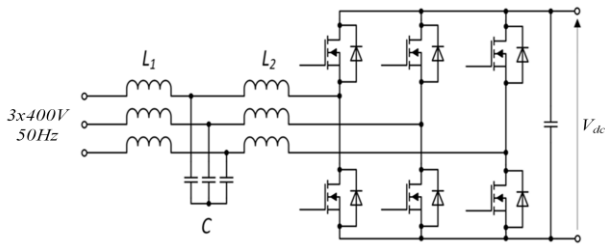| Parameter	Symbol	Value
Phase voltage of the grid	V_{ac}	3x230 V
Maximum DC voltage	V_{dc}	800 V
Nominal apparent power	S	10 kVA
Range of power factor change	λ	$0.7 \div 1.0$
Relative ripple of DC voltage	$\Delta V_{dc\%}$	5%
Total harmonic distortion of current	THD_i	5%
RMS value of rated current	I_{rms}	15 A
Minimum switching frequency	f_{sw}	40 kHz

Fig. 1. Circuit model of the PWM converter with MOSFET switches

A. Control System

In the first stage of simulation tests, the correctness of the control system operation was verified. The main task of the control algorithm is stabilization of output voltage V_{dc} around a reference value while controlling the value of power factor λ at the same time. Moreover, sinusoidal modulation of voltage pulses on the AC side of the converter is provided.
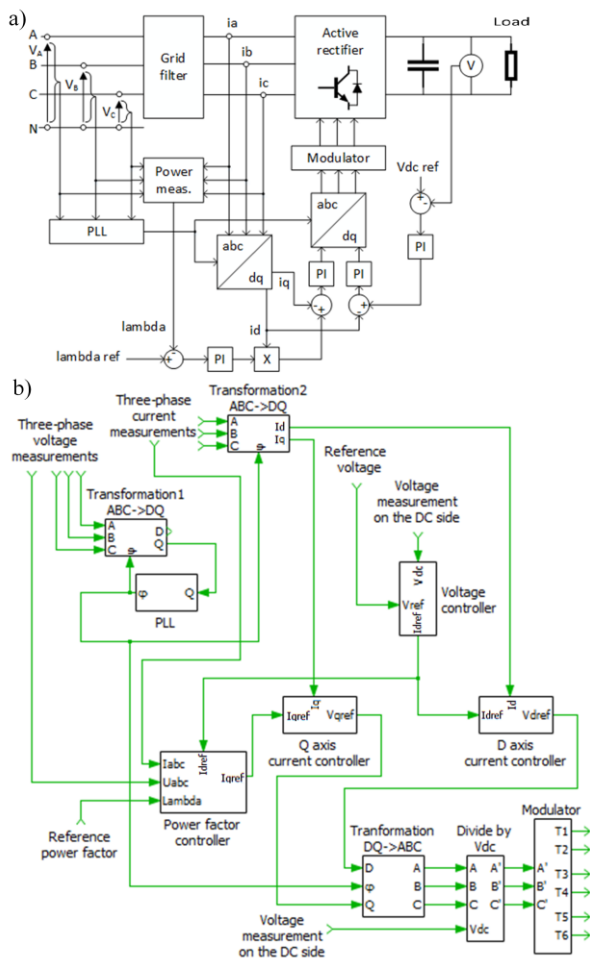

Fig. 2. Control system with direct power factor regulation: block diagram (a) and its implementation in a simulation model (b)

The control algorithm uses the transformation of measurement signals from three-phase system to the rotating reference system d-q, which allows the use of simple PI regulators (Fig. 2) [16]. The transformation of three-phase voltages and currents to the d–q system is provided by the blocks abc -> dq. In each such block, in addition to signals proportional to the instantaneous values of phase currents or voltages, a value of the angle φ between current and voltage waveforms, obtained from phase-locked loop (PLL), is applied

[17].

After determining the RMS values of voltage (V_{rms}) and current (I_{rms}) and average value of apparent (S) and active (P) power, the power factor $\lambda = P / S$ is calculated, which, assuming only a slight distortion of the grid current ($THD_i < 5\%$), is approximately equal to the value of $\cos\phi$. In the adopted control algorithm the power factor is influenced by changes in the passive component of the grid current vector - I_q. The setpoint value of this component determines the value of the power factor. On the other hand, the V_{dc} voltage regulator acts on the active component I_d of the grid current vector, which is proportional to the active power P taken from the grid.

To check the operation of the power factor control algorithm, a simulation was performed, in which the reference value of the power factor was changed from 1.0 to 0.8 (at constant active power value P = 6 kW). The proposed algorithm was written using C-script block to most accurately reflect the operation of a real digital controller. Results of this study, presented in Fig. 3, confirm the theoretical analysis and correct operation of the control algorithm.
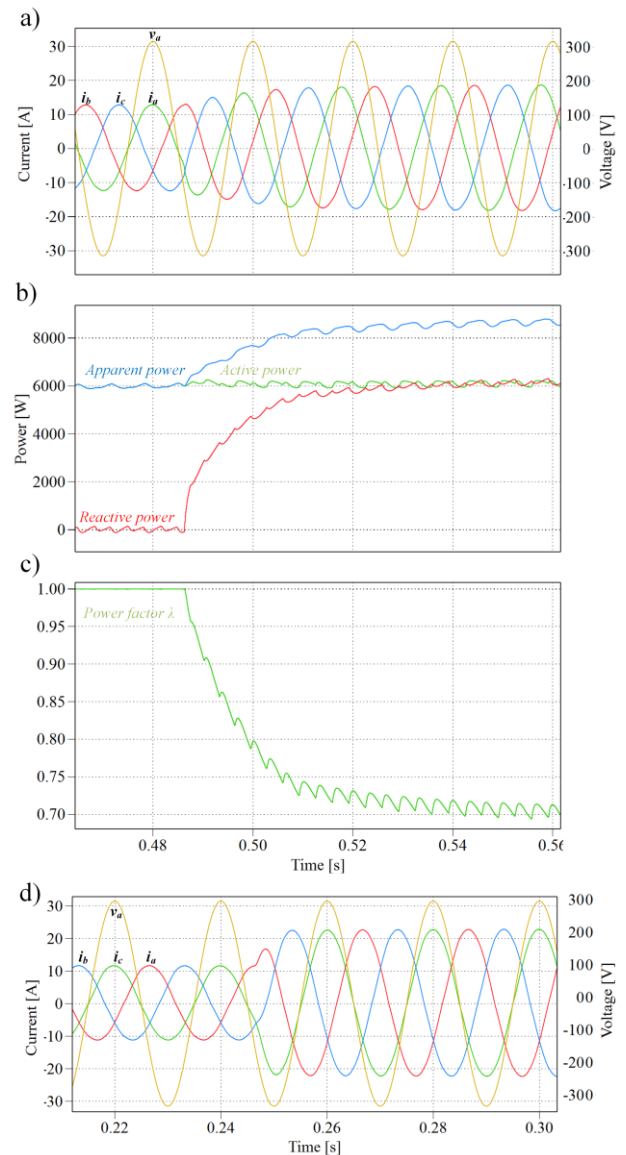

Fig. 3. Results of the operation of the converter during step change of the power factor (a-c) and step change of the load resistance (d) – simulation studies

B. Design of AC and DC filters

The study of a simplified converter simulation model with ideal semiconductor switches also showed correct operation of the space vector modulator (SVM). The control algorithm provides a sinusoidal shape of waveforms of the AC grid currents, which depends not only on the modulation method, but also on the switching frequency (f_s = 40 kHz) and the type of the grid filter (Fig. 4). In order to select the filter parameters, grid current THD_i minimization (less than 5%) as well as minimization of geometrical dimensions, power losses and costs were all taken into account. Literature analysis [18] and simulation study have shown that these criteria are best met by the filter according to Fig. 4c with 1.8 mH < L_1 < 6 mH; C = 1.5 µF; L_2 = 150 µH, meeting the condition of $10f < f_{rez} < 0.5f_{sw}$, where f = 50 Hz and

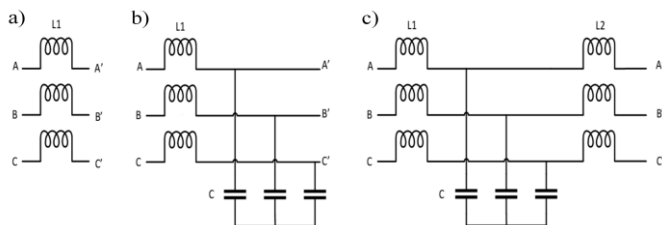$$f_{rez} = \frac{1}{2\pi}\sqrt{\frac{L_1+L_2}{L_1 L_2 C}} \tag{1}$$

Fig. 4. Alternate filter versions on the AC line side: (a) L filter; (b) LC filter; c) LCL filter

When selecting DC filter capacitors, it was assumed that the peak-to-peak ripple value of the output voltage $\Delta V_{dc\%}$ should be below 5% of the average value of this voltage. Simulation tests have shown that in addition to the DC filter capacitance, switching frequency and the load current, the distortion and asymmetry of the supply grid currents have influence on the value of $\Delta V_{dc\%}$. A slight dependence between ripple $\Delta V_{dc\%}$ and the deadtime between PWM signals was also observed. Multilateral simulation tests for the nominal conditions allowed to determine the final value of DC capacitance as C_{DC} = 1 mF.

C. Semiconductor Components

When choosing diodes and transistors, typical criteria were adopted, including: maximum blocking voltages (1200 V), permissible current carrying capacity (I_{Trms} > 15 A), minimization of conduction (diodes: P_{C-D}, transistors: $P_{C-MOSFET}$ and P_{C-IGBT}) and switching (diodes: P_{SW-D}, transistors: $P_{SW-MOSFET}$; $P_{SW-IGBT}$) power losses. Initial analysis of available semiconductor devices allowed to select switches (transistors with free-wheeling diodes) with the following designations: SK35GD126ET and SKiiP25AC12F4V19 (IGBT); SCT3080KL, C2M0040120D and LSIC1M0120E0080 (MOSFET SiC). In order to determine the power losses dissipated in the semiconductor switches, a simulation model of the converter was built and tested, and the obtained results were used to calculate power losses based on the following formulas:

$$P_{C\_IGBT} = V_{CE0}I_{AV\_T} + r_T I_{RMS\_T}^2 \tag{2}$$

$$P_{C\_MOSFET} = r_T I_{RMS\_T}^2 \tag{3}$$

$$P_{C\_D} = V_{F0}I_{AV\_D} + r_D I_{RMS\_D}^2 \tag{4}$$

$$P_{SW\_IGBT} = f_{SW}(E_{ON} + E_{OFF})I_{AV\_T}/I_{RMS\_T} \tag{5}$$

$$P_{SW\_MOSFET} = f_{SW}V_{dc}I_{RMS\_T}(t_{ON} + t_{OFF}) \tag{6}$$

$$P_{SW\_D} = f_{SW}E_{rec}I_{AV\_D}/I_{RMS\_D} \tag{7}$$

where: V_{CE0}, V_{F0} - threshold voltage values of the IGBT transistor and the diode; I_{AV-T}, I_{AV-D} - average values of transistor and diode currents; I_{RMS-T}, I_{RMS-D} - effective values of transistor and diode currents; E_{ON}, E_{OFF} - energy loss caused by switching the component on and off; E_{rec} - loss of energy when switching off the diode; r_T, r_D - transistor and diode resistance in the conduction state.

In addition, a thermal model of the converter was developed, in which a special thermal library of transistors was implemented, taking into account the characteristics of energy loss as a function of voltage and current. The results of analytical calculations and simulation tests are presented in Table II.
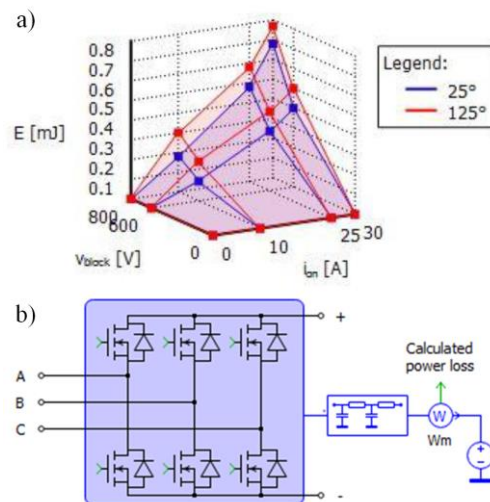

Fig. 5. Implementation of energy loss characteristics to the thermal model of the transistor (a) and thermal model of the converter in PLECS (b)

TABLE II
COMPARISON OF POWER LOSSES [W] IN SiC MOSFETs

Model Transistor	P_{C_D}	P_{C_T}	P_{SW_D}	P_{SW_T}	Total	Simul. results
SCT3080KL	185.6	12.15	14	51.84	263.6	230
SK35GD126ET	100.5	9.72	44.5	34.56	189.2	150
SKIIP25ACF4V19	49.73	52.1	109.9	104.9	316.6	- [a]
C2M0040120D	117.1	10.85	44.49	98.4	270.8	155
LSIC1MO120E008	181	12.15	20.6	22.46	236.2	190

[a]No simulation model.

III. EXPERIMENTAL MODEL

Based on the assumptions and calculations. the design of the converter was developed. whose three-dimensional model is shown in Fig. 6a. Fig. 6b shows the experimental model of the prototype of a 10 kVA grid converter with MOSFET SiC. The power density factor was reached at the level of 5.2 kW / dm³.
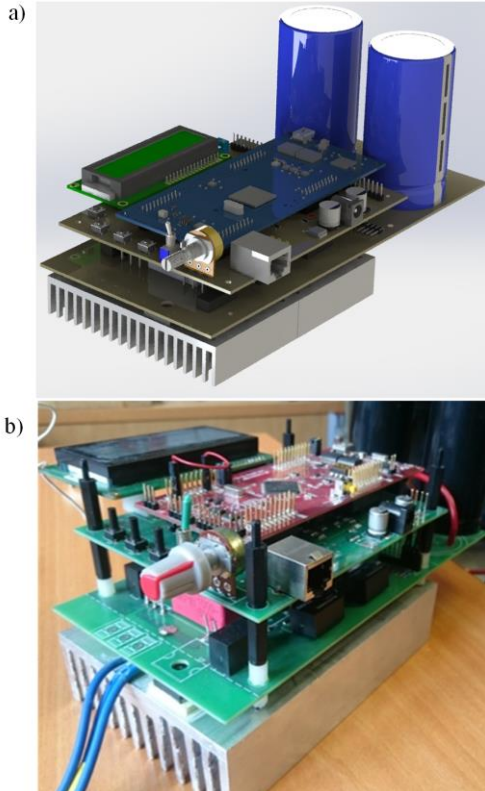

Fig. 6. Three-dimensional model (a) and experimental model (b) 10kVA PWM rectifier based on SiC MOSFETs
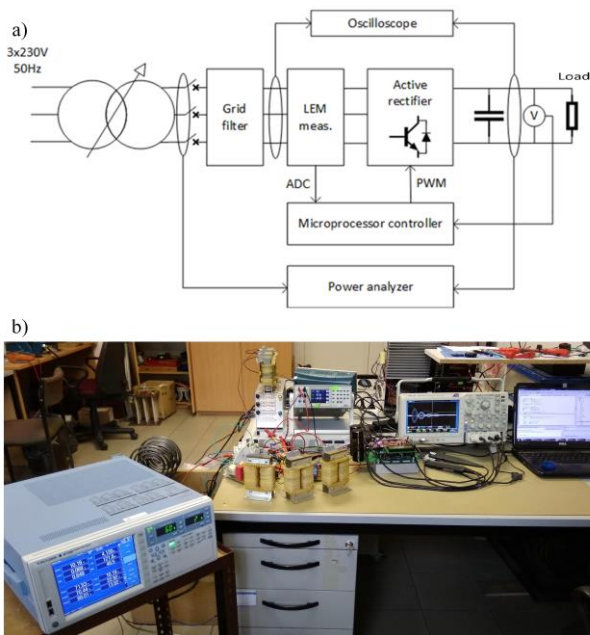

Fig. 7. Block diagram (a) of the test bench and a view at the converter's experimental setup (b)

To implement the control system. a Texas Instruments TMS320F28377S microcontroller was used. in which a control algorithm verified in simulation model was implemented. Its main task was generation of six independent PWM signals. which were connected to the inputs of gate drivers through optical isolation (Silicon Labs SI8127). SiC transistors were controlled using bipolar gate voltage (-5 V to + 20 V) supplied from dedicated small isolated DC/DC converters (Murata MGJ2D242005SC). In order to limit the charging and discharging current of the transistor input capacitance. an additional resistor in the gate circuit of 4.3Ω is used.

The main circuit of the converter was made using six SiC MOSFETs LSIC1M0120E0080 [19] and an AC filter in the L_1-C-L_2 configuration. where $L_1 = 0.5 \div 6$ mH. $C = 1.5$ µF. $L_2 = 150$ µF. The target L_1 and L_2 inductance values were selected based on experiments performed at different loads. The DC filter was composed of two parallel sections of 1-mF / 550-V capacitors connected in series due to limited maximum voltage rating of these capacitors. Fig. 7 shows a block diagram and a picture of the experimental setup.

A. Starting the system in inverter mode

First of all. the system was started in inverter mode. in which the load was made from symmetrical arrangement of R-L elements connected in a star. with $\omega L >> R$. The inverter DC bus was supply from an adjustable laboratory power supply 0-650V. Next. using the oscilloscope and precise measuring probes. the instantaneous voltage and current values of the transistor were measured during turn on and turn off switching time. The purpose of the observations was to confirm the correct operation of the control circuits. as well as to evaluate the dynamic properties of these power switches and to verify the characteristics of energy losses as a function of voltage and current. implemented in the simulation model. Sample oscillograms are presented in the Fig. 8.
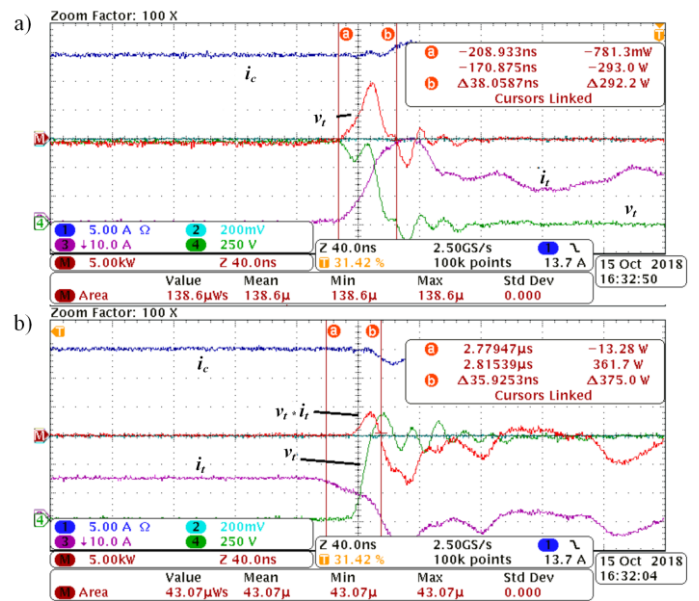

Fig. 8. Instantaneous voltage v_{ds}. drain current i_d and power $p_{sw} = v_{ds}i_d$ of the SiC MOSFET during turn on (a) and turn off (b); $V_{dc} = 600$ V. $I_{rms} = 15$ A
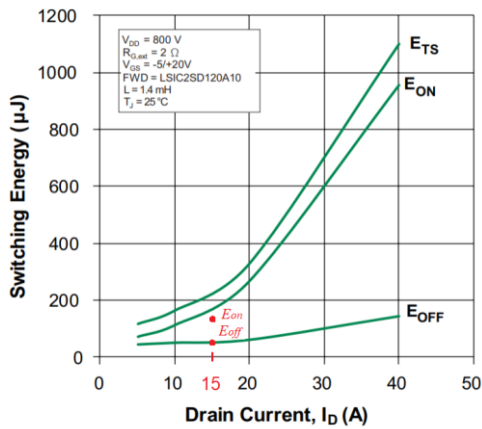
Fig. 9. Switching energy vs drain current characteristic for LSIC1M0120E0080 MOSFET [18]. (red – measured energy for $V_{dc} = 600V$)

As can be seen in Fig. 8 and Fig. 9. the recorded values of the switching on and off energy of the SiC transistor coincide with values declared in the manufacturer datasheet [19]. This also confirms the correctness of the data for the thermal model of the SiC transistor in simulation tests.

B. Converter power losses - experimental measurements

The power losses of PWM rectifier were determined as the difference between the active power obtained from the grid and the power measured at the DC side. To estimate power losses of the converter. input and output power values were measured for different switching frequencies. Based on these measurements. conduction and switching power losses was calculated. Assuming that the conduction losses in the converter (P_c = 55W) are independent of the switching frequency. the converter losses can be separated from losses in the grid filter.

TABLE III
RESULTS OF THE EXPERIMENTAL POWER LOSSES MEASUREMENTS

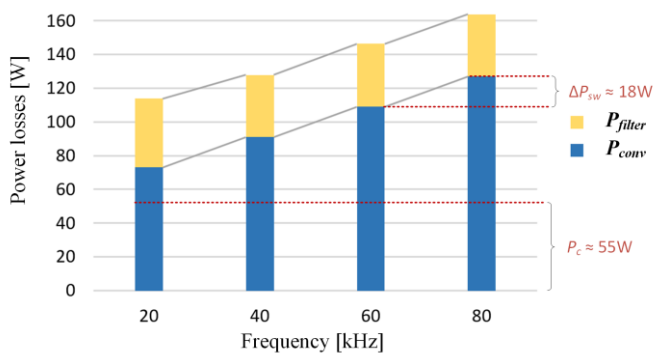| Switching frequency [kHz]	20	**40**	60	80
Total power losses [W]	113.8	**127.9**	146.3	163.7
Power losses in the converter [W]	73	**91**	109	127
Power losses in grid filter [W]	40.8	**36.9**	37.3	36.7

Fig. 10. Power losses in PWM rectifier with LCL filter for different switching frequencies at 6kW

Results of the experimental measurements of the converter power losses for P = 6 kW for different switching frequencies. were presented in Table III and Fig. 10.

The obtained results indicate that with use of L_1 = 6 mH. THD_i is less than 2% and the energy efficiency of the converter at P = 6 kW and f_{sw} = 40 kHz is around 98.5% (Fig. 11)
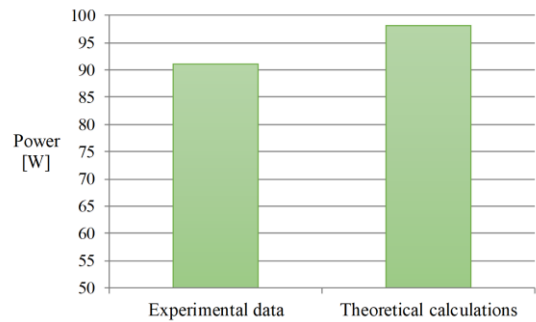

Fig. 11. Experimental and theoretical results of total power losses in the PWM rectifier at active power value P = 6 kW. f_{sw} = 40 kHz

C. Power quality and control system dynamics tests

The measurements of THD_i coefficient for different grid filter configurations were conducted using Yokogawa WT1800 power analyzer (Fig. 12). Three LCL filter configurations were used for the tests. in which the value of L_1 inductors (0.5 mH. 1.8 mH and 6 mH) was changed. The results of the THD_i measurements of the grid current are shown in Fig. 11. It shows that even with 1.8 mH inductance the requirements of standards regarding the content of higher harmonics are met (below 5%).
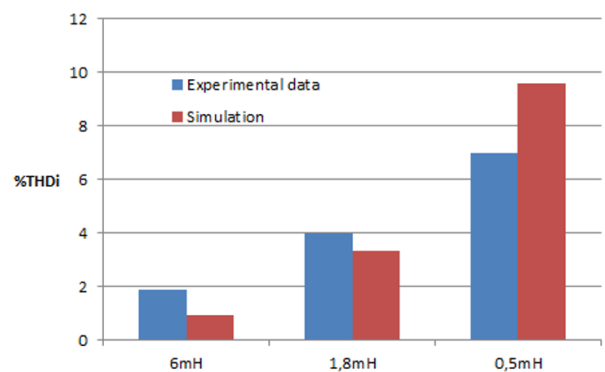

Fig. 12. THD$_i$ factor of the line current for different values of inductance L_1 of the AC filter L_1-C-L_2

Experimental tests were also carried out to determine the compensating properties of the converter (Fig. 13) and dynamics of the control system (Fig. 14). Presented waveforms confirm correct operation of the converter and control system. which implements all design assumptions.

IV. CONCLUSIONS

A full research cycle is presented. the result of which is the design. construction and testing of an experimental three-phase model (3x400 V / 50 Hz) of a 10-kW PWM converter built with silicon carbide MOSFETs. selected from the ever richer offer of these elements. The use of PLECS simulation program and the C-language algorithm significantly improves the implementation of the control system realized using a fast DSP microcontroller. Thanks to the use of fast SiC transistors switched at 40 kHz. it was possible to obtain instantaneous grid currents with very low harmonic distortion values (THD_i < 2%) at small dimensions of the grid filter. According to the

assumptions. in the load range of up to 10 kVA the converter can fulfill not only the function of a power supply (with bi-directional energy flow). but also that of a reactive power compensator. The results of measurements of power losses dissipated in the whole system show a far-reaching convergence with the analytical results and simulation calculations and confirm the high energy efficiency of the tested system (98.5%). Great practical advantages of the PLECS program. which offers the possibility of creating thermal profiles of semiconductor devices and easy selection of heat sinks. have been confirmed.
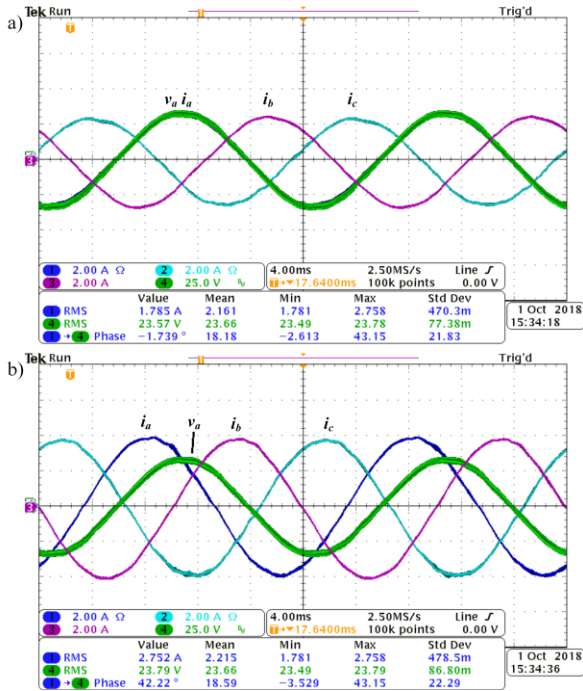

Fig. 13. Grid voltage and current waveforms at unity power factor (a) and phase shift between voltage v_a and grid current i_a for $\lambda = 0.7$ (b)
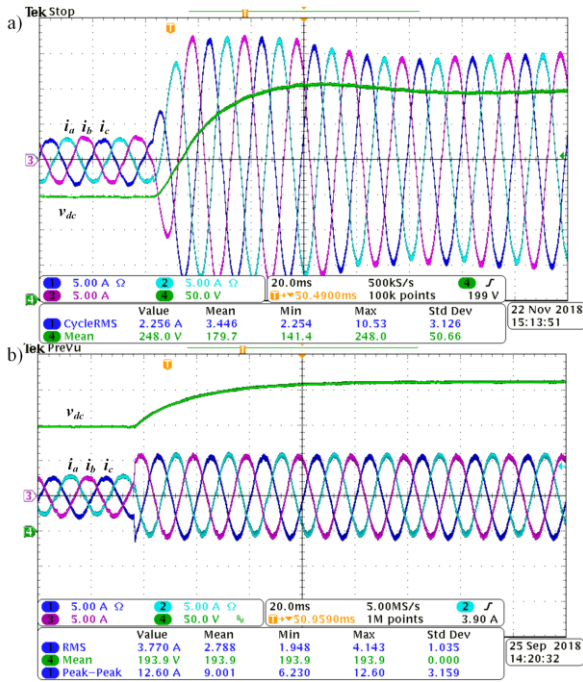

Fig. 14. DC voltage v_{dc} and grid current waveforms at step changes of reference DC voltage value (a) and reference power value (b)

REFERENCES

[1] J. C. Balda and A. Mantooth. "Power-Semiconductor Devices and Components for New Power Converter Developments: A key enabler for ultrahigh efficiency power electronics." in *IEEE Power Electronics Magazine*. vol. 3. no. 2. pp. 53-56. June 2016.

[2] F. F. Wang and Z. Zhang. "Overview of silicon carbide technology: Device. converter. system. and application." in *CPSS Transactions on Power Electronics and Applications*. vol. 1. no. 1. pp. 13-32. Dec. 2016.

[3] S. Piasecki and J. Rąbkowski. "The 10 kVA SiC-based grid connected AC/DC converter with extended functionalities — Experimental investigation." *2016 10th International Conference on Compatibility. Power Electronics and Power Engineering (CPE-POWERENG)*. Bydgoszcz. 2016. pp. 214-218.

[4] F. Xu. B. Guo. L. M. Tolbert. at all. "Evaluation of SiC MOSFETs for a high efficiency three-phase buck rectifier." *27th Annual IEEE Appl. Power Electr.Conf. and Exp. (APEC)*. Orlando. FL. 2012. pp. 1762-1769.

[5] A. Kouchaki and M. Nymand. "Efficiency Evaluation of Three-phase SiC Power Factor Correction Rectifier with Different Controllers." *2018 20th European Conference on Power Electronics and Applications (EPE'18 ECCE Europe)*. Riga. 2018. pp. P.1-P.10.

[6] A. Stupar. T. Friedli. J. Minibock at all. "Towards a 99% Efficient Three-Phase Buck-Type PFC Rectifier for 400-V DC Distribution Systems." in *IEEE Trans. on Power Electr.*. vol. 27. no. 4. pp. 1732-1744. 2012.

[7] S. Wall. X. Hong. L. Sha and J. Xie. "High-efficiency PV inverter with SiC technology." in *IET Renewable Power Generation*. vol. 12. no. 2. pp. 149-156. 2018.

[8] B. Zhao. Q. Yu. and W. Sun. "Wide-band gap devices in PV systems opportunities and challenges." *IEEE Transactions on Power Electronics*. vol. 27. no. 11. pp. 4667–4680. Nov 2012

[9] S. Hamasaki. K. Nakahara and M. Tuji. "Harmonics Compensation in High Frequency Range of Active Power Filter with SiC-MOSFET Inverter in Digital Control System." *2018 International Power Electronics Conference*. Niigata. 2018. pp. 3237-3242.

[10] D. Kranzer. J. Thoma. B. Volzer. D. Derix and A. Hensel. "Development of a 10 kV three-phase transformerless inverter with 15 kV Silicon Carbide MOSFETs for grid stabilization and active filtering of harmonics." *2017 19th European Conference on Power Electronics and Applications (EPE'17 ECCE Europe)*. Warsaw. 2017. pp. P.1-P.8.

[11] S. Madhusoodhanan et al.. "Solid-State Transformer and MV Grid Tie Applications Enabled by 15 kV SiC IGBTs and 10 kV SiC MOSFETs Based Multilevel Converters." in *IEEE Transactions on Industry Applications*. vol. 51. no. 4. pp. 3343-3360. July-Aug. 2015.

[12] J. E. Huber. J. Böhler. D. Rothmund and J. W. Kolar. "Analysis and cell-level experimental verification of a 25 kW all-SiC isolated front end 6.6 kV/400 V AC-DC solid-state transformer." in *CPSS Transactions on Power Electronics and Applications*. vol. 2. no. 2. pp. 140-148. 2017.

[13] A. Khaligh and M. D'Antonio. "Global Trends in High-Power OnBoard Chargers for Electric Vehicles." in *IEEE Transactions on Vehicular Technology*. vol. 68. no. 4. pp. 3306-3324. April 2019.

[14] C. Jiang. B. Lei. H. Teng and H. K. Bai. "The power-loss analysis and efficiency maximization of a silicon-carbide MOSFET based three-phase 10kW bi-directional EV charger using variable-DC-bus control." *2016 IEEE Energy Conversion Congress and Exposition (ECCE)*. Milwaukee. WI. 2016. pp. 1-6.

[15] Grzejszczak P.. „ Methodology for determining power losses in switching devices of dual active bridge converter with taking into account the thermal effects". *PhD thesis*. Warsaw University of Technology. 2014.

[16] M. Malinowski. M. Jasinski and M. P. Kazmierkowski. "Simple direct power control of three-phase PWM rectifier using space-vector modulation (DPC-SVM)." in *IEEE Transactions on Industrial Electronics*. vol. 51. no. 2. pp. 447-454. April 2004.

[17] W. Phips W.. M. J. Harrison and R. M. Duke. „Three-Phase Phase-Locked Loop Control of a New Generation Power Converter." *2006 1ST IEEE Conf. on Ind.Electr. and Appl.*. Singapore. 2006. pp.1-6.

[18] C. Nardi. C. M. Stein. E. G. Carati. at all.."A methodology of LCL filter design for grid-tied Power converters". *IEEE 13th Brazilian Power Electron. and 1st Southern Power Electron. Conf.*. Fortaleza. 2015.

[19] Datasheet MOSFET SiC LSIC1M0120E0080. online: *https://www.littelfuse.com* (2019)